30th Congress of the International Council of the Aeronautical Sciences
DCC, Daejeon, Korea ; September 25-30, 2016

OPTIMAL APPROACH TRAJECTORIES FOR MULTIPLE AIRCRAFT CONSIDERING DISTURBANCES AND CONFIGURATION CHANGES

M. Bittner, M. Rieck, B. Grüter, F. Holzapfel,
Institute of Flight System Dynamics, Technische Universität München, Germany

Keywords: Air Traffic Management, Trajectory Optimization, Conflict Resolution, Optimal Control, Discrete Decisions.

Abstract

In the paper at hand, cost-index-optimal trajectories for multiple aircraft approaching an airport in the presence of wind disturbances are calculated. The optimization is based on optimal control techniques using the full trapezoidal discretization scheme implemented in FALCON.m[1] *[1], and the gradient based numerical optimization software* IPOPT *[2]. The main result presented here is a modeling technique and a multi stage solution process for large scale trajectory optimization problems from the field of ATM. In the first stage of this process, each trajectory is optimized individually, before afterwards multiple problems for an increasing number of aircraft are solved. Finally, optimal trajectories for all aircraft in the scenario result, that adhere to the flight envelopes and separation limits while minimizing the total cost index summed up over all aircraft in the scenario. The aircraft dynamics are simulated using point mass simulation models in three dimensional space with the aerodynamics and the fuel flow models taken from the Base of Aircraft Data Family 4 (BADA 4) published by EUROCONTROL [3]. The considered scenario – part of the approach to Tokyo International Airport – is based on real trajectories extracted from* MLIT CARATS Open Data *published by the* Japanese Ministry of Land, Infrastructure, Transport and Tourism. *Besides, the scenario includes the influence of wind, modeled based on data from the* Earth System Research Laboratory. *In the scenario, the optimal state and control histories for 18 aircraft as well as the optimal points in time for deploying the flaps are determined. The inherent discrete decision problem of sequencing the aircraft is automatically solved by the numerical optimization algorithm in parallel to the calculation of the trajectories. The optimization stops prior to the final approach fix.*

1 Introduction

Currently, many big research projects like *SESAR* or *NextGen* focus on the development of the future ATM system. The goal of all these endeavors is to extensively reorganize the air traffic systems in order to bring safety and capacity to the next level. The results of this paper show what can currently be achieved in ATM when using the high perfor-

Matthias Rieck holds a scholarship of Munich Aerospace e.V.

[1] https://www.falcon-m.com

mance optimal control techniques of tools like *FALCON.m* in combination with a strong numerical optimization algorithm like *IPOPT*.

The main challenge when solving problems like the one presented here is to achieve convergence of the numerical optimization. Here, a two step approach is used: First, the trajectories for all aircraft are optimized individually, anyway already considering wind and the discrete switching for the flaps. Afterwards, the aircraft are one by one added to the overall problem, starting the solution process of each problem with the solution for the optimization variables as well as the *Lagrange* multipliers (dual variables) of the previous problem.

The calculation of optimal trajectories for multiple aircraft has received some attention during the last couple of years. In [4] a problem very similar to the one presented here has been solved, using a comparable method. However, in the problem solved in the present work, wind disturbances are added and the aircraft configuration changes by means of high lift devices are incorporated in the problem formulation. Moreover, now 18 aircraft are considered, compared to nine in the previous work. Even before, Fisch presented the solution to a multi aircraft optimization problem including four aircraft in [5]. In [6] a fairness assessment for scenarios including several aircraft has been performed. In the calculations, trajectories for multiple aircraft have been optimized for the costs of each single aircraft as well as the combination of costs for all aircraft.

In the papers [7, 8, 9, 10] different scenarios with a total of four to eight aircraft of very different model fidelity are considered. They are solved by various different optimization methods ranging from *Rapidly Exploring Random Tree Algorithms* to *Optimal Control* and *Mixed Integer (Non)linear Programming*. Moreover, they show different approaches for modeling obstacles and separation constraints.

The remainder of this paper is structured as follows: Section 2 describes the dynamic model for simulating each single aircraft under the influence of wind. Next, section 3 gives an overview of the optimal control problem formulation and the techniques used to solve it. The specific formulation of a multi aircraft problem and the multi stage solution strategy is described in section 4. The results created in the example scenario are described in section 5. Finally, some conclusions are drawn and an outlook is given in section 6.

2 Aircraft Simulation Model

A three-degree-of-freedom (3-DoF) aircraft simulation model is used here with the aerodynamics, the fuel flow model, and other aircraft specific information taken from the *Base of Aircraft Data Family 4 (BADA4)* published by EUROCONTROL [3]. The simulation includes wind, resulting in different values for the kinematic and the aerodynamic quantities in the model. The model is controlled by the lift coefficient, the bank angle and the thrust lever position. Besides, the spoiler deflection is considered as a model input. The flaps position, which may be seen as a discrete control, is handled using a hyperbolic tangent parameterized by the time of extraction, which eventually is a continuous variable. More details the flaps modeling can be found in section 2.6.

Table 1 Aircraft States and Controls

Name	State	Unit
x	x-position in locally fixed frame	m
y	y-position in locally fixed frame	m
z	z-position in locally fixed frame	m
V_K	kinematic velocity	m/s
χ_K	kinematic course angle	rad
γ_K	kinematic climb angle	rad
m	aircraft mass	kg

Name	Control	Unit
C_L	lift coefficient	-
μ_K	kinematic bank angle	rad
δ_T	thrust lever (normalized)	-
δ_{SB}	speed brake (normalized)	-

Overall, the resulting dynamic system for one aircraft features seven states and four controls, as listed in Table 1. The following subsections give a brief overview of the subsystems included in the model.

2.1 Position Equations of Motion

The position vector is given in a Locally Fixed Frame N that is derived from the North-East-Down (NED) Reference Frame O with its x-axis pointing northward, its y-axis eastward and its z-axis downward, but fixed to a point on the surface of the earth, close to the destination airport:

$$\begin{pmatrix} \dot{x} \\ \dot{y} \\ \dot{z} \end{pmatrix}_N^E = \begin{pmatrix} V_K \cdot \cos\chi_K \cdot \cos\gamma_K \\ V_K \cdot \sin\chi_K \cdot \cos\gamma_K \\ -V_K \cdot \sin\gamma_K \end{pmatrix}_N \tag{1}$$

In this model, the earth is considered to be flat and non-rotating.

2.2 Translation Equations of Motion

The derivatives of the kinematic velocity V_K, the kinematic course angle χ_K, and the kinematic flight path inclination angle γ_K are depending on the forces acting on the aircraft. Denoted with respect to the Kinematic Reference Frame K and using L for the aerodynamic lift, D for the drag, and g for gravity, the following equations result:

$$\begin{aligned} \dot{V}_K &= \frac{T-D}{m} - g \cdot \sin\gamma_K \\ \dot{\chi}_K &= \frac{L \cdot \sin\mu_K}{m \cdot V_K \cdot \cos\gamma_K} \\ \dot{\gamma}_K &= \frac{L \cdot \cos\mu_K}{m \cdot V_K} - \frac{g \cdot \cos\gamma_K}{V_K} \end{aligned} \tag{2}$$

2.3 Wind

In general, the aerodynamic velocity required for the calculation of aerodynamic forces can be derived from the kinematic velocity using the wind equation:

$$(\mathbf{V}_A)_O^E = (\mathbf{V}_K)_O^E - (\mathbf{V}_W)_O^E \tag{3}$$

The derivative of the wind speed, that is required in the path constraints described in section 2.7 is calculated from:

$$\begin{aligned} &(\dot{\mathbf{V}}_A)_O^E = (\dot{\mathbf{V}}_K)_O^E - \\ &\left(\left(\frac{\partial}{\partial t}\right)^O (\mathbf{V}_W)_O^E + \nabla^O (\mathbf{V}_W)_O^E \cdot (\mathbf{V}_K)_O^E \right) \end{aligned} \tag{4}$$

In the example, the wind field is modeled to be time invariant and only depending on the current air pressure, which changes with altitude – no changes in the lateral extent are considered. The wind distribution is an approximation of the *Twentieth Century Reanalysis (V2)* wind data from the *Earth System Research Laboratory*. Based on a the daily mean wind for the region around Tokyo International Airport, polynomial wind models of sixth order for northward and eastward wind speeds have been derived by interpolation. The wind speeds are modeled as:

$$\begin{aligned} V_{W,u/v} = {} & p_1 \cdot (p_H)^6 + p_2 \cdot (p_H)^5 \\ & + p_3 \cdot (p_H)^4 + p_4 \cdot (p_H)^3 \\ & + p_5 \cdot (p_H)^2 + p_6 \cdot p_H + p_7 \end{aligned} \tag{5}$$

with the numerically normalized pressure altitude p_H being defined as:

$$p_H = \frac{p - 442.9\ \text{mbar}}{327.9\ \text{mbar}} \tag{6}$$

This normalization does not have any physical meaning but is only necessary for numerical reasons. For February 3rd, 2012 the polynomial coefficients given in Table 2 result. The pressure is calculated from the current flight altitude of each aircraft based on the *International Standard Atmosphere (ISA)* [11].

Table 2 Coefficients of the approximation polynomials for the wind speed [m/s]

Coefficient	Eastward wind (u)	Northward wind (v)
p_1	−3.409	1.584
p_2	12.950	−0.08236
p_3	−15.310	−9.390
p_4	1.831	−1.133
p_5	20.220	20.750
p_6	−41.320	−2.118
p_7	37.700	−7.854

2.4 Force Equations

The aerodynamic forces are calculated as described in the *BADA* documents [3]. Besides others, the forces depend on the Mach number M, the current speed of sound a, the adiabatic index κ, the universal gas constant R, and the current air temperature T that are all calculated according to the *ISA*. The required aerodynamic quantities are calculated from the kinematic states using the wind equation (3).

2.5 Fuel Flow Modeling

The fuel flow model is taken from the *BADA* data, resulting in a differential equation for the mass:

$$\dot{m} = -\dot{m}_{fuel}(m, p, T, M, \delta_T) \tag{7}$$

2.6 Configuration Changes

The extension of the flaps, representing a configuration change of the aircraft, is modeled using a function based on a hyperbolic tangent expressions for each position s of the flaps that is considered. The main influencing parameter is the point in time $t_{\text{flaps},s}$ when the switching takes place. This parameter is mapped to the relative extension of the considered position $k_{\text{flaps},s} \in [0, 1]$ by:

$$k_{\text{flaps},s} = 0.5 \cdot \tanh(t - t_{\text{flaps},s}) + 0.5 \tag{8}$$

Within the model, the value for any exemplary aerodynamic parameter p_A is calculated by fading between the parameters for the different positions (e.g. clean and s_1) of the flaps while the extension is performed:

$$p_A = p_{A,\text{clean}} + (p_{A,\text{flaps},s_1} - p_{A,\text{clean}}) \cdot k_{\text{flaps},s_1} \tag{9}$$

In the example presented below, besides the clean configuration, two flap configurations have been selected for each aircraft.

2.7 Path Constraints

Along the whole trajectories, the following path constraints have to hold: The load factor in z-direction of the Kinematic Frame K is limited to:

$$0.8 \le (n_z)_K \le 1.2 \tag{10}$$

The *Mach number* is limited by:

$$M \le 0.85 \tag{11}$$

All aircraft need to be decelerating reasonably all the time by means of calibrated airspeed:

$$-0.8\frac{m}{s^2} \le \dot{V}_{CAS} \le 0\frac{m}{s^2} \tag{12}$$

The vertical speed of the aircraft is limited to approximately $-2500\frac{ft}{min}$ and needs to be negative:

$$-13\frac{m}{s} \le \dot{h} = -\dot{z} \le 0\frac{m}{s} \tag{13}$$

The set of admissible controls for each aircraft is defined by:

$$\begin{aligned}
0 &\le C_L \le 1.4 && (14)\\
-30 \cdot \frac{\pi}{180} &\le \mu_K \le 30 \cdot \frac{\pi}{180} && (15)\\
0 &\le \delta_T \le 1 && (16)\\
0 &\le \delta_{SB} \le 1 && (17)
\end{aligned}$$

3 Applied Optimal Control

In general, a multi aircraft trajectory optimization problem involving N aircraft may be stated as follows:
Determine the optimal control histories

$$\mathbf{u}_{i,opt}(t) \in \mathbb{R}^m, \qquad i = 1, ..., N, \tag{18}$$

the required additional parameters

$$\mathbf{p}_{i,opt} \in \mathbb{R}^q, \qquad i = 1, ..., N \tag{19}$$

and the optimal state trajectories

$$\mathbf{x}_{i,opt}(t) \in \mathbb{R}^n, \qquad i = 1, ..., N \tag{20}$$

that minimize the Bolza cost functional

$$J = \sum_{i=1}^{N} \left[e_i(\mathbf{x}_i(t_{f,i}), t_{f,i}) + \int_{t_{0,i}}^{t_{f,i}} L_i(\mathbf{x}_i(t), \mathbf{u}_i(t), t)dt \right] \tag{21}$$

subject to the state dynamics

$$\dot{\mathbf{x}}_i = \mathbf{f}_i(\mathbf{x}_i, \mathbf{u}_i, \mathbf{p}_i), \qquad i = 1, ..., N \tag{22}$$

the initial and final boundary conditions

$$\begin{aligned}
\boldsymbol{\psi}_{0,i}(\mathbf{x}_i(t_{0,i}), t_{0,i}) &= \mathbf{0}, \qquad i = 1, ..., N && (23)\\
\boldsymbol{\psi}_{f,i}(\mathbf{x}_i(t_{f,i}), t_{f,i}) &= \mathbf{0}, \qquad i = 1, ..., N && (24)
\end{aligned}$$

and the equality and inequality conditions

$$\begin{aligned} \mathbf{C}_{eq,i}(\mathbf{x}_i(t), \mathbf{u}_i(t), t) &= \mathbf{0} \\ \mathbf{C}_{ineq,i}(\mathbf{x}_i(t), \mathbf{u}_i(t), t) &\leq \mathbf{0} \\ i = 1, ..., N & \end{aligned} \tag{25}$$

For solving this problem the direct *Trapezoidal Collocation Scheme* of *FALCON.m* has been used, that can e.g. also be found in [12].

3.1 Gradient Calculation

After discretizing the optimal control problem, a huge numerical optimization problem needs to be solved. Here, the gradient based, Interior Point software IPOPT [2], designed for sparse problems, has been used for this purpose, with all required gradients calculated analytically by *FALCON.m*. In order to achieve this, the local gradients of the simulation model and all constraints with respect to the states, the controls and the parameters are automatically calculated using the *Symbolic Math Toolbox* from *MATLAB*. In case of complicated simulation models, it is required to construct them from several subsystem functions, that are derived before the resulting code is automatically coupled together within the tool using the chain rule (for more details, see [13]). Finally, everything required to evaluate the model dynamics and the constraints of the problem (including all gradients) is compiled into a fast running *MATLAB Executable (mex)* using *MATLAB Coder*. More details can also be found in the user guide of *FALCON.m* [1].

4 Multi Aircraft Optimization

Here, the mathematical modeling and the solution process of a multi aircraft optimization problem containing N aircraft are described.

4.1 Combined Dynamic Model

In order to be able to compare the position of all aircraft at the same points in time, a simulation on one common grid is inevitable. The overall optimal control problem is modeled in one single phase, aggregating all aircraft dynamics in one simulation model. As not all aircraft enter or leave the considered air space at the same time, the respective dynamics are faded in or out using a hyperbolic tangent function:

$$\dot{\mathbf{x}}_i = \mathbf{f}_i(\mathbf{x}_i, \mathbf{u}_i, \mathbf{p}_i) \cdot k_{\text{fade}} \tag{26}$$

$$\begin{aligned} k_{\text{fade}} = &\left(0.5 \cdot \tanh\left(\nu\left(t - t_{i,ini}\right)\right) + 0.5\right) \\ &\cdot \left(-0.5 \cdot \tanh\left(\nu\left(t - t_{i,end}\right)\right) + 0.5\right) \end{aligned} \tag{27}$$

By changing ν, the steepness of the fading functions is adjusted. In the example shown below, $\nu = 1$ is used. As the time when the aircraft enter the considered airspace is known, the initial times $t_{i,ini}$ are fixed while the final times $t_{i,end}$ are subject to optimization. The same fading is used for the path constraints.

The state, control, and parameter vectors of the multi aircraft optimization problem are a combination of the respective vectors for each single aircraft:

$$\mathbf{x} = (\mathbf{x}_1, \mathbf{x}_2, ..., \mathbf{x}_N)^\intercal \tag{28}$$

$$\mathbf{u} = (\mathbf{u}_1, \mathbf{u}_2, ..., \mathbf{u}_N)^\intercal \tag{29}$$

$$\mathbf{p} = (\mathbf{p}_1, \mathbf{p}_2, ..., \mathbf{p}_N)^\intercal \tag{30}$$

The same holds for the dynamic equation:

$$\begin{aligned} \dot{\mathbf{x}} = \mathbf{f}(\mathbf{x}, \mathbf{u}, \mathbf{p}) = &(\mathbf{f}_1(\mathbf{x}_1, \mathbf{u}_1, \mathbf{p}_1), \\ &\mathbf{f}_2(\mathbf{x}_2, \mathbf{u}_2, \mathbf{p}_2), ..., \\ &\mathbf{f}_N(\mathbf{x}_N, \mathbf{u}_N, \mathbf{p}_N))^\intercal \end{aligned} \tag{31}$$

The price to pay for the simulation on the common grid is the size of the resulting simulation model which contains seven states and four controls *per* aircraft in the scenario. Anyway, the gradient of the simulation model features a special sparsity structure.

4.2 Separation

In addition to the path constraints for every single aircraft specified in section 2, temporal and spatial separation between the aircraft has to be ensured. The times of arrival at the final point considered of each pair of aircraft are constrained by:

$$(t_{i,end} - t_{j,end})^2 \geq {t_{\min Sep}}^2, \ \forall (i,j), i \neq j \tag{32}$$

with $t_{\min Sep} = 60s$. Besides, the spatial distance between each pair of aircraft, modeled as a rotational ellipse, has to remain above the separation limit:

$$\begin{aligned}(x_i(t) - x_j(t))^2 + (y_i(t) - y_j(t))^2 \\ + \left(\frac{R_{xy}}{R_z}\right)^2 \cdot (z_i(t) - z_j(t))^2 \geq {R_{xy}}^2 \\ \forall (i,j), i \neq j\end{aligned} \quad (33)$$

The radius R_{xy} in the horizontal plane is selected depending on the aircraft weight classes (H–H:$R_{xy} = 4NM = 7408m$, M–M: $R_{xy} = 3NM = 5556m$, M–H/H–M: $R_{xy} = 5NM = 9260m$) while the vertical separation $R_z = 600ft = 183m$ is constant for all combinations.

4.3 Cost Function

The cost function to be minimized consists of three weighted parts, being

- the fuel consumption,
- the flight times,
- and a small auxiliary term penalizing the control effort during the faded-out parts of the trajectories.

The last part is required as otherwise the controls in the faded-out parts would not influence the optimization problem at all, resulting in undefined values for the solution. The fuel consumption is calculated from the initial and the final masses by

$$J_{fuel} = \sum_{i=1}^{N} (m_{i,ini} - m_{i,end}) \quad (34)$$

The time cost is calculated from

$$J_{time} = \sum_{i=1}^{N} t_{i,end} \quad (35)$$

where the initial times may be omitted as they are constant anyway. The scaling of the two cost functions is selected such that a cost index

$$CI = \frac{1\text{cost}/1000sec}{1\text{cost}/100kg} = 6\frac{kg}{min} \quad (36)$$

results. This very low cost index results in almost fuel minimal trajectories.

The control effort is modeled as

$$J_{con} = \sum_{i=1}^{N} \int_{t_{ini}}^{t_{end}} \mathbf{u}_i(t)^\intercal \mathbf{u}_i(t) \cdot (1 - k_{\text{fade}})\, dt \quad (37)$$

with k_{fade} being the fading factor from equation (27). The auxiliary control cost is weighed by $w_{Jcon} = 0.01$ and does not influence the relevant part of the solution.

4.4 Sparsity

The model dynamics are block-diagonal sparse because of the different dynamic models being concatenated together. *FALCON.m* determines the sparsity structure of a model and all constraints automatically before supplying this information to the numerical solver. Figure 1 shows the local sparsity of the simulation model where the first block represents the gradient of the state derivative with respect to the states $\frac{\partial \dot{\mathbf{x}}}{\partial \mathbf{x}}$, the second part shows the gradient with respect to the controls $\frac{\partial \dot{\mathbf{x}}}{\partial \mathbf{u}}$ and the third part represents the gradient with respect to the parameters $\frac{\partial \dot{\mathbf{x}}}{\partial \mathbf{p}}$, being the fade in time $t_{i,ini}$ and the fade out time $t_{i,end}$.

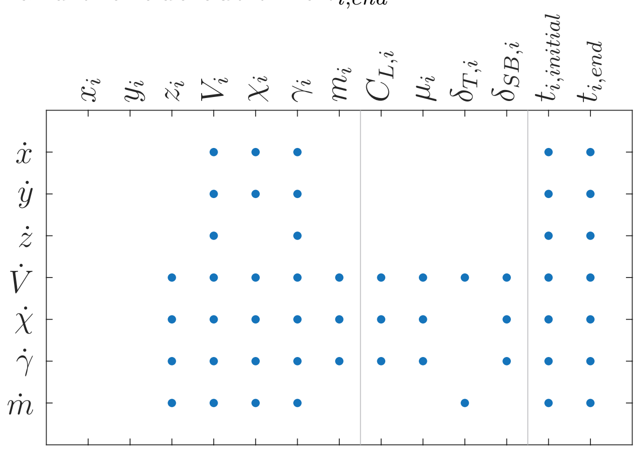

Fig. 1 Combined local sparsity pattern for the gradient of the simulation model $[\frac{\partial \dot{\mathbf{x}}}{\partial \mathbf{x}} \frac{\partial \dot{\mathbf{x}}}{\partial \mathbf{u}} \frac{\partial \dot{\mathbf{x}}}{\partial \mathbf{p}}]$.

Each block along the diagonal of the combined simulation model features the structure depicted in figure 1. The gradient structure of the path constraints can be constructed similarly, except for the separation constraints, that create dependencies between the aircraft.

4.5 Solution Process

The combined optimal control problem ensuring separation at all times cannot be directly solved due to its high nonlinearity and its large size. Therefore, the following multi-stage process is used:

1) Solve the approach problem for each aircraft individually.
2) Add the aircraft to the fully constrained problem one after the other, until all aircraft are considered.

In each optimization step, the states, controls, parameters and all *Lagrange* multipliers (dual variables) for the collocation defects and the constraints are used as the initial guess for the next problem to be solved.

5 Results

The scenario considered in this study focuses on an approach to Tokyo International Airport and has been constructed using *MLIT CARATS Open Data* released by the Japanese Civil Aviation Bureau of the Ministry of Land, Infrastructure, Transport and Tourism (*MLIT JCAB*). Thereof, track data from the 4^{th} of March 2013 in the time between noon and 6 o'clock in the evening has been used. From this data, 18 tracks have been extracted for constructing the scenario. Table 3 lists the 18 flights that have been considered together with the aircraft types and the initial positions. The wind speeds resulting from the model derived from the data from the *Earth System Research Laboratory* within the relevant area lie in the range of $8m/s$ to $70m/s$ eastward and $-8m/s$ to $5m/s$ northward.

In figure 2 the resulting optimal tracks for all aircraft can be seen. They are mostly straight lines as this is the most time and fuel efficient way to go. Almost all arising conflicts can be solved within the optimization by adjusting the vertical profiles and the velocities along the tracks. Only one aircraft is rerouted by the optimization algorithm in or-

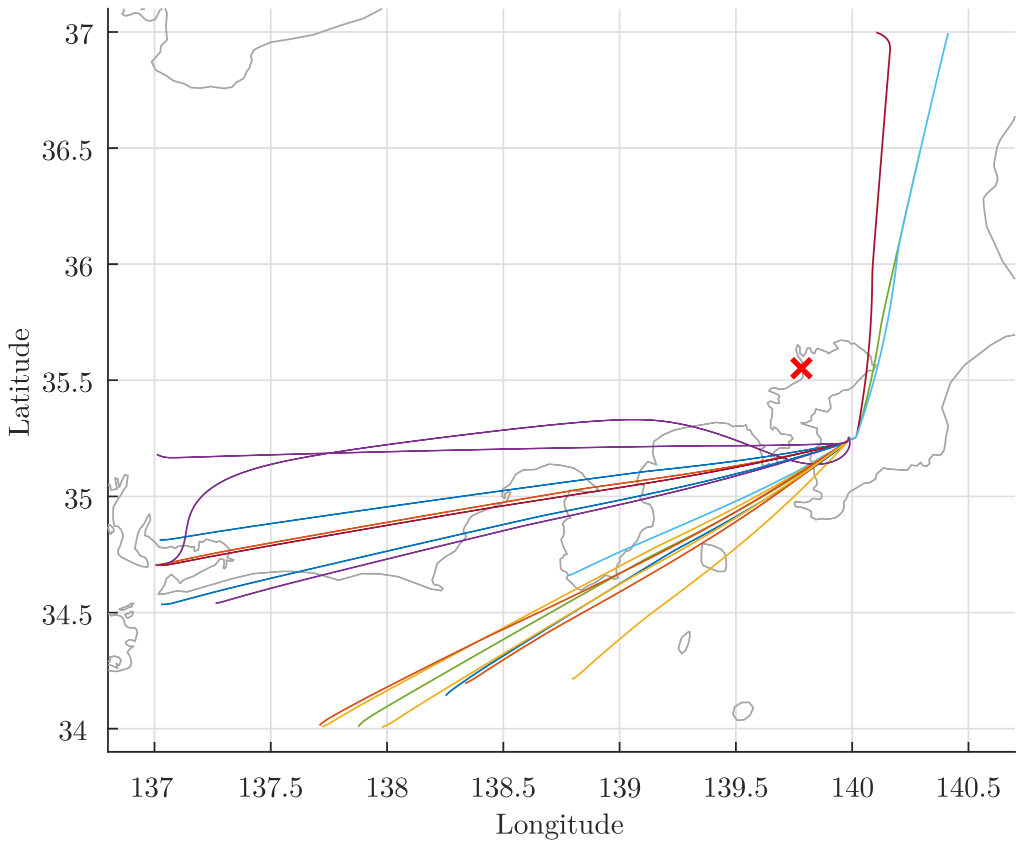

Fig. 2 Optimal trajectories for all aircraft. Tokyo International Airport is marked with the cross.

Table 3 Data for the aircraft and the trajectories in the example scenario.

AC Type	Weight Cat	Start Lat [deg]	Start Lon [deg]	Start Altitude [m]	Start Time [s]	Final Time [s]	Flap Time [s]
B738W26	M	34.1419	138.2522	8440	0	1420	-
A330-341	H	34.1947	138.3352	10020	0	1266	1238
B738W26	M	34.2130	138.7952	8530	0	1125	-
B772LR	H	34.5399	137.2626	10659	1	1645	-
B738W26	M	36.4880	140.2920	4916	2	1065	-
B772LR	H	34.6585	138.7760	8564	9	835	445
B738W26	M	36.9979	140.1037	7010	23	1360	-
A321-131	M	34.8133	137.0220	10058	33	1820	-
B752WRR40	M	34.7052	137.0034	11278	308	2145	-
B738W26	M	34.0073	137.7211	10052	493	2085	-
B738W26	M	34.7028	137.0076	10659	515	2740	-
B73423	M	34.0081	137.8762	10355	562	2025	-
A320-231	M	36.9949	140.4129	7910	569	1960	-
B738W26	M	34.7031	137.0272	12490	594	2221	-
B772LR	H	34.5353	137.0278	11271	869	2661	-
B763ERGE61	H	34.0140	137.7094	12497	1005	2601	-
B738W26	M	34.0067	137.9777	10058	1024	2431	-
B772LR	H	35.1811	137.0097	8120	1384	3171	-

der to ensure final time separation. At this point the main weakness of the algorithm becomes visible as (with every gradient based approach) only local minima can be found and it is not known whether rerouting a different aircraft would probably lead to another (maybe even better) locally optimal solution. Moreover, other solutions may be found by changing the way the initial guesses are calculated or by changing the solution process described in section 4.5. The small arcs in the trajectories of the aircraft coming from the north are related to the partially strong eastward wind and its dependence on the flight altitude.

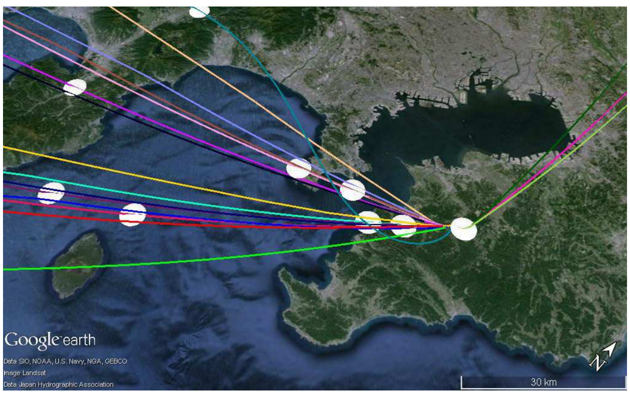

Fig. 3 Final part of the trajectories and separation ellipsoids for the aircraft at one point in time.

Figure 3 shows a close-up of the last part of the trajectories. Therein, the tracks of all aircraft are visualized in *Google Earth* and the positions at one point in time is plotted. The white ellipsoids have a diameter of $3NM$ being the minimum required separation between two aircraft of weight category M. For these aircraft the ellipsoids may not interfere along the whole trajectories.

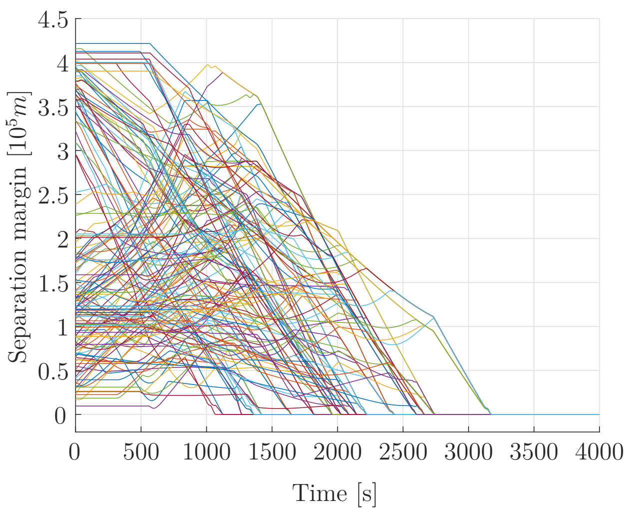

Fig. 4 Separation margin between all pairs of aircraft over time.

As all aircraft in the scenario have to keep separation distances pairwise to each other, for the considered scenario comprising 18 aircraft, a total of $N \cdot (N-1)/2 = 153$ separation constraints result. Thus, the number of separations grows quadratically with the number of aircraft making it far more difficult to solve a problem with 18 aircraft compared to one with e.g. 9 in the work [4]. The number of separation distance constraints is equal to the number of final time constraints in the problem, even though the distance constraints need to be applied in every time step, while the final time separation only adds one overall constraint per aircraft pairing. The remaining separation margins for all pairs of aircraft, that need to be positive, can be seen in figure 4. For some constellations the margin is hit but it is never violated.

The last column of Table 3 lists the optimal extraction times for the first considered position of the flaps for every aircraft. As can be seen, only the second and the sixth aircraft use their flaps in the considered part of the trajectory to create more lift at lower speeds. For all other aircraft the use of the flaps is neither necessary nor does it create a benefit in the overall cost. This is reasonable as the increased lift of the flaps comes for the price of an also increased drag which raises the fuel burn as well as the required time to the destination.

In this example, the simulation model in the final problem contained $18 \cdot 7 = 126$ states and $18 \cdot 4 = 72$ controls, both discretized on a grid with 801 points in time. Overall, the numerical optimization problem contained 158,634 optimization variables and 295,615 constraints. The gradient matrix, consisting of the cost function gradient and the constraint Jacobian, comprised 2,911,140 structural nonzero elements resulting in a sparsity ratio of 99.9938%.

6 Conclusions

This paper presents a specially tailored modeling approach together with a two step solution method for solving large scale optimal control problems involving multiple aircraft. The considered example scenario comprises 18 aircraft approaching Tokyo International Airport in parallel. The optimization is based on a 3-DoF simulation model in three dimensional space. The aircraft specific parameters as well as the aerodynamic and fuel consumption models have been taken from the *BADA Family 4* dataset.

The problem is formulated as an optimal control problem that is discretized using the direct collocation approach implemented in *FALCON.m*. The resulting numerical optimization problem is solved using *IPOPT*. The main challenge is to achieve convergence of the highly nonlinear large scale optimal control problem that requires to fully exploit the problem inherent sparsity properties as well as the creation of good initial guesses which is assured by the two step approach.

The results show how cost-index-optimized continuous-descent operations in a highly congested airspace, like the one in the proximity of a strongly frequented airport, may look like. The required aircraft performance envelope as well as the separation limits are thereby maintained at all times. Anyway, controller workload and coordination of the different aircraft is not considered here and may put some additional constraints to such a scenario.

Overall, the method and the solution presented here is (at the moment) not intended as an approach for improving the daily work of ATC controllers. The method and the study is much more suitable to provide a means of benchmarking different solutions for future ATM systems against this optimal solution.

The solution of the problems discussed in this paper takes a lot of computational time and the method does not show a general stable behavior when adding more aircraft. This is on the one side related to the mere problem size which is hard to tackle using *IPOPT*. This may be overcome by using special large scale solvers like e.g. *WORHP* [14]. On the other side, the addition of further aircraft lets the number of pairwise separation constraints grow even more which at some point will eventually limit this method.

Moreover, the fact that gradient based optimization algorithms can only find local minima (which may be global) results in the fact that there may exist other solutions that deliver better performance than the one found, which cannot be determined as they are located in another “valley” of the solution space. This may be especially problematic when the discrete decisions like the sequencing in the problems described here become crucial.

In order to overcome these aforementioned drawbacks, a hybrid optimization process may be used that separates the problem of determining the optimal trajectory for one aircraft from the optimization of the sequencing and the ensuring of the separations. Different methods may be used within the two levels of the resulting problem, possibly also overcoming the issue of converging to local minima in the sequencing problem.

7 Contact Author Email Address

m.bittner@tum.de

Copyright Statement

References

[1] Matthias Rieck, Matthias Bittner, Benedikt Grüter, and Johannes Diepolder. Falcon.m user guide.

[2] Andreas Wächter and Lorenz T. Biegler. On the implementation of a primal-dual interior point filter line search algorithm for large-scale nonlinear programming. *Mathematical Programming*, 106(1):25–57, 2006.

[3] Eurocontrol Experimental Centre. User manual for the base of aircraft data (bada) family 4.

[4] Matthias Bittner, Matthias Rieck, Benedikt Grüter, and Florian Holzapfel. Optimal conflict free approach trajectories for multiple aircraft. In *ENRI Int. Workshop on ATM/CNS (EIWAC2015)*, 2015.

[5] Florian Fisch, Matthias Bittner, and Florian Holzapfel. Optimal scheduling of fuel-minimal approach trajectories. *Journal of Aerospace Operations*, 2014.

[6] Matthias Bittner, Benjamin Fleischmann, Maximilian Richter, and Florian Holzapfel. Optimization of atm scenarios considering overall and single costs. In *6th International Conference on Research in Air Transportation*, 2014.

[7] Krithika Mohan, Michael A. Patterson, and Anil V. Rao. Optimal trajectory and control generation for landing of multiple aircraft in the presence of obstacles. In *28th International Congress Of The Aeronautical Sciences*, 2012.

[8] Arvind U. Raghunathan, Vipin Gopal, Dharmashankar Subramanian, Lorenz T. Biegler, and Tariq Samad. Dynamic optimization strategies for three-dimensional conflict resolution of multiple aircraft. *Journal of Guidance, Control, and Dynamics*, 27(4):586–594, 2004.

[9] A. Richards and J. P. How. Aircraft trajectory planning with collision avoidance using mixed integer linear programming. In *Proceedings of the 2002 American Control Conference*, pages 1936–1941 vol.3, [Piscataway, NJ], 2002. IEEE.

[10] Tom Schouwenaars, Jonathan How, and Eric Feron. Decentralized cooperative trajectory planning of multiple aircraft with hard safety guarantees. In *AIAA Guidance, Navigation, and Control Conference and Exhibit*, [Reston, Va.], 2004. [American Institute of Aeronautics and Astronautics].

[11] DIN ISO 2533:1979-12. Standard atmosphere.

[12] John T. Betts. *Practical Methods for Optimal Control and Estimation Using Nonlinear Programming*. Society for Industrial and Applied Mathematics, Philadelphia, 2009.

[13] Matthias Rieck, Matthias Bittner, Benedikt Grüter, and Florian Holzapfel. Generation of dynamic models with automatically generated derivatives for atm optimal control in matlab. In *ENRI Int. Workshop on ATM/CNS (EIWAC2015)*, 2015.

[14] Christof Büskens and Dennis Wassel. The esa nlp solver worhp. In Giorgio Fasano and János D. Pintér, editors, *Modeling and Optimization in Space Engineering*, volume 73 of *Springer Optimization and Its Applications*, pages 85–110. Springer New York, 2013.